IX International Conference on Computational Methods for Coupled Problems in Science and Engineering
COUPLED PROBLEMS 2021
E. Oñate, M. Papadrakakis and B. Schrefler (Eds)

UNCERTAINTY QUANTIFICATION OF AN AUTONOMOUS SURFACE VEHICLE BY MULTI-FIDELITY GAUSSIAN PROCESS

S. FICINI[1,2], R. PELLEGRINI[2], A. ODETTI[2], A. SERANI[2], U. IEMMA[1], M. CACCIA[2], AND M. DIEZ[2]

[1]Roma Tre University, Department of Engineering, Italy
e-mail: simone.ficini@uniroma3.it

[2]CNR-INM, National Research Council-Institute of Marine Engineering, Italy
e-mail: matteo.diez@cnr.it

Key words: Uncertainty Quantification, Multi-Fidelity Gaussian Process, Adaptive Sampling, Autonomous Surface Vehicle

Abstract. A multi-fidelity Gaussian process (MF-GP) is presented for the forward uncertainty quantification (UQ) of the performance of an autonomous surface vehicle (ASV) subject to uncertain operating conditions. The ASV is a shallow water autonomous multipurpose platform (SWAMP), designed for the acquisition of the environmental parameters in the extremely shallow waters of wetlands. The quantity of interest (QoI) is the hydrodynamic resistance of the SWAMP subject to variable payload and longitudinal position of its center of mass. The QoI is assessed by a linear potential-flow solver coupled with the rigid body equations of motion. Multiple fidelity levels are defined based on the computational grid size and the level of coupling between hydrodynamic loads and motions. The MF-GP is based on a low-fidelity surrogate, corrected with an additive function, representing the error between higher and lower fidelity solutions. The MF-GP provides the prediction with the associated uncertainty. The latter is used to adaptively train the MF-GP, adding points where the prediction uncertainty is maximum. Finally, the UQ of the QoI is performed by Monte Carlo sampling on the MF-GP surrogate. The first four statistical moments, the 95th percentile, and the probability density function of the QoI are assessed. MF-GP is compared to its single-fidelity (high-fidelity based) counterpart, showing overall better results.

1 INTRODUCTION

The operation planning of aerial, ground, and marine vehicles requires the accurate prediction of their performance, to guarantee the success of the mission and the safety during

the operations. The accurate prediction of the performance usually requires physics-based high-fidelity solvers, especially for off-design conditions and innovative configuration, which may produce non-linear responses or complex multi-physics interactions (*e.g.*, plastic deformation of structures or hydroelasticity). High-fidelity solvers are generally computationally expensive, making the exploration of the uncertain parameters space a technological challenge. To reduce the computational cost of the uncertainty quantification (UQ) process, multi-fidelity (MF) surrogate models have been developed [1]. A MF surrogate model exploits the possibility of using several fidelities, using different solvers and/or the same solver with different space/time discretization, as well as different coupling level between several disciplines. Among other MF methods, co-Kriging [2] and Gaussian process (GP) [3] have been successfully applied in several engineering fields. To further reduce the computational cost of exploring the uncertain parameters space, adaptive sampling methods can be used [4]. These methods aim to add training points for the MF surrogate only where they are more informative, exploiting the information that becomes available during the UQ process.

The objective of the present work is the assessment of a MF-GP surrogate model for the forward UQ of the performance of an autonomous surface vehicle (ASV) with uncertain operating conditions. The ASV is a shallow water autonomous multipurpose platform (SWAMP) designed for the acquisition of the environmental parameters in the extremely shallow waters of wetlands [5]. The quantity of interest (QoI) is the hydrodynamic resistance of the SWAMP subject to variable payload and longitudinal position of its center of mass. Both the uncertain parameters follow a uniform distribution.

The QoI is assessed by multi-disciplinary/multi-fidelity simulations. Specifically, an in-house linear potential-flow solver coupled with the rigid body equations of motion [6] is used. Three fidelity levels are defined based on the computational grid size and the level (tightness) of the coupling between hydrodynamic loads and motion. The MF-GP is built as a low-fidelity trained surrogate model corrected with the surrogate of the errors between successive fidelities. The MF-GP training sets are dynamically updated with an adaptive sampling method based on the maximum uncertainty associated to the MF-GP prediction. The adaptive sampling method automatically selects the fidelity to sample, balancing between the maximum prediction uncertainty and the computational cost associated to each fidelity level [7]. The UQ of the QoI is achieved applying a Monte Carlo (MC) sampling on the MF-GP surrogate model. The UQ provides the probability density function (PDF) of the QoI, whose accuracy is evaluated by the Kolmogorov-Smirnov (KS) test against a high-fidelity benchmark. Furthermore, the relative errors of the first four statistical moments and the 95th percentile are reported. Finally, the performance of the MF-GP is compared to its single-fidelity (high-fidelity based) counterpart.

2 MULTI-FIDELITY GAUSSIAN PROCESS

The following subsections describe the single-fidelity GP, its MF extension, and, finally, the adaptive sampling procedure.

2.1 Gaussian Process

Given a training set $\mathcal{T} = \{\mathbf{x'}_i, f(\mathbf{x'}_i)\}_{i=1}^{J}$, where $\mathbf{x'} \in \mathbb{R}^D$ is the parameters vector of dimension D and J the training set size, normalizing the parameters domain into a unit hypercube, the GP prediction $\widetilde{f}(\mathbf{x})$ with constant mean and its variance $\mathrm{Var}[\widetilde{f}(\mathbf{x})]$ can be written as [8]

$$\begin{aligned} \widetilde{f}(\mathbf{x}) &= \mathbb{E}[\mathbf{f}(\mathbf{x'})] + \mathbf{k}(\mathbf{x},\mathbf{x'})\mathbf{K}(\mathbf{x'},\mathbf{x'})^{-1}(\mathbf{f}(\mathbf{x'}) - \mathbb{E}[\mathbf{f}(\mathbf{x'})]), \\ \mathrm{Var}[\widetilde{f}(\mathbf{x})] &= \mathbf{K}(\mathbf{x},\mathbf{x}) - \mathbf{k}(\mathbf{x},\mathbf{x'})^{\mathsf{T}}\mathbf{K}(\mathbf{x'},\mathbf{x'})^{-1}\mathbf{k}(\mathbf{x},\mathbf{x'}), \end{aligned} \tag{1}$$

where $\mathbb{E}[\mathbf{f}(\mathbf{x'})]$ is the expected value of $\{f(\mathbf{x'}_i)\}_{i=1}^{J}$, $\mathbf{K}(\mathbf{x'},\mathbf{x'})$ is the covariance matrix with elements $K_{ij} = k(\mathbf{x}'_i, \mathbf{x}'_j)$, and $\mathbf{k}(\mathbf{x},\mathbf{x'})$ is the covariance vector with elements $k_i = k(\mathbf{x}, \mathbf{x}'_i)$. Finally, $k(\cdot,\cdot)$ is the covariance function defined as [8]

$$k(\mathbf{x},\mathbf{x'}) = \sigma_F^2 \exp\left(-\boldsymbol{\gamma}^{\mathsf{T}}(\mathbf{x}-\mathbf{x'})^{\circ 2}\right) + \sigma_n^2\delta(\mathbf{x},\mathbf{x'}), \tag{2}$$

with "$\circ$" the Hadamard product, $\delta(\mathbf{x},\mathbf{x'})$ the Kronecker delta, and $\boldsymbol{\Lambda} = \{\sigma_n^2, \sigma_F^2, \boldsymbol{\gamma}\}$ the set of the GP hyper-parameters [8]. Specifically, σ_n^2 is the variance associated to the noise in the training set, σ_F^2 is the signal variance, and $\boldsymbol{\gamma} \in \mathbb{R}^D$ is the vector of the inverse length scale parameters. It can be noted that the use of the parameter σ_n^2 leads to a regressive formulation of the GP. The hyper-parameters are evaluated by maximizing the log marginal likelihood l [8] as follows

$$\boldsymbol{\Lambda}^\star = \{\sigma_n^{2,\star}, \sigma_F^{2,\star}, \boldsymbol{\gamma}^\star\} = \underset{\sigma_n^2,\sigma_F^2,\boldsymbol{\gamma}}{\mathrm{argmax}}[l], \tag{3}$$

with

$$l = \log\left[p(f(\mathbf{x'})|\mathbf{x'})\right] = -\frac{J}{2}\log 2\pi - \frac{1}{2}f(\mathbf{x'})^{\mathsf{T}}\mathbf{K}(\mathbf{x'},\mathbf{x'})^{-1}f(\mathbf{x'}) - \frac{1}{2}\log|\mathbf{K}(\mathbf{x'},\mathbf{x'})|. \tag{4}$$

The uncertainty $U_{\widetilde{f}}$, associated to the surrogate model prediction, is here quantified as

$$U_{\widetilde{f}} = 4\sqrt{\mathrm{Var}[\widetilde{f}(\mathbf{x})]}. \tag{5}$$

It may be noted, that the present definition of $U_{\widetilde{f}}$ incorporates the variance associated to the noise in the training set.

2.2 Multi-fidelity Approach

Considering a QoI that can be evaluated with N fidelity levels (where the first level is the highest-fidelity and the N-th level is the lowest-fidelity) the MF extension of the GP is built as follows [9]. Given a training set $\mathcal{T}_i = \{\mathbf{x'}_j, f_i(\mathbf{x'}_j)\}_{j=1}^{J_i}$ for $i = 1, \ldots, N$, the MF approximation $\hat{f}_i(\mathbf{x})$ of $f_i(\mathbf{x})$ is defined as

$$\widehat{f}_i(\mathbf{x}) := \widetilde{f}_N(\mathbf{x}) + \sum_{k=i}^{N-1}\widetilde{\varepsilon}_k(\mathbf{x}), \tag{6}$$

where $\widetilde{\varepsilon}_k(\mathbf{x})$ is the inter-level error surrogate with an associate training set $\mathcal{E}_k = \{(\mathbf{x'}_i, f_k(\mathbf{x'}_i) - \widehat{f}_{k+1}(\mathbf{x'}_i)) \,|\, \mathbf{x'}_i \in \mathcal{T}_k \cap \mathcal{T}_{k+1}\}_{i=1}^{J_k}$. Assuming the uncertainty associated to the prediction of the lowest-fidelity $U_{\widetilde{f}_N}$ and inter-level errors $U_{\widetilde{\varepsilon}_k}$ as uncorrelated, the MF approximation $\widehat{f}_1(\mathbf{x})$ of $f_1(\mathbf{x})$ and the associated uncertainty $U_{\widehat{f}_1}$ read

$$f_1(\mathbf{x}) \approx \widehat{f}_1(\mathbf{x}) = \widetilde{f}_N(\mathbf{x}) + \sum_{k=1}^{N-1} \widetilde{\varepsilon}_k(\mathbf{x}), \qquad \text{and} \qquad U_{\widehat{f}_1}(\mathbf{x}) = \sqrt{U^2_{\widetilde{f}_N}(\mathbf{x}) + \sum_{k=1}^{N-1} U^2_{\widetilde{\varepsilon}_k}(\mathbf{x})}. \quad (7)$$

2.3 Adaptive Sampling

The MF surrogate is iteratively updated adding new training points following an adaptive sampling procedure. First, the coordinates of the new training point $\mathbf{x}^\star$ are identified based on the maximum uncertainty prediction [7], solving the single-objective maximization problem

$$\mathbf{x}^\star = \underset{\mathbf{x}}{\text{argmax}}[U_{\widehat{f}_1}(\mathbf{x})]. \quad (8)$$

Second, once $\mathbf{x}^\star$ is identified, the training set $\mathcal{T}_i$ is updated with the new training point $(\mathbf{x}^\star, f_i(\mathbf{x}^\star))$ with $i = k, \ldots, N$, where k is defined as

$$k = \text{maxloc}\left[\mathbf{V}(\mathbf{x}^\star)\right], \qquad \text{with} \qquad \mathbf{V} \equiv \begin{Bmatrix} (\text{Var}[\widetilde{\varepsilon}_1] - \sigma^{2,\star}_{n,\widetilde{\varepsilon}_1} - p_1)/\beta_1 \\ \vdots \\ (\text{Var}[\widetilde{\varepsilon}_{N-1}] - \sigma^{2,\star}_{n,\widetilde{\varepsilon}_{N-1}} - p_{N-1})/\beta_{N-1} \\ (\text{Var}[\widetilde{f}_N] - \sigma^{2,\star}_{n,f_N} - p_N)/\beta_N \end{Bmatrix} \quad (9)$$

where β_i is the computational cost associated to the i-th fidelity level (normalized with respect to the high-fidelity one) and p_i is a penalization value. The latter is used to avoid over-fitting of the training points, which would result in an ill-conditioned matrix while solving Eqs. 1 and 3. The penalization p_i is applied only if $\mathbf{x}^\star$ lies within a minimum distance $d_{\min}$ of an already existing training point of $\mathcal{T}_i$. In such a case p_i is evaluated as

$$p_i = \sum_{j=1}^{J_i} \frac{1}{\|\mathbf{x}^\star - \mathbf{x}'_j\| + \tau}, \quad (10)$$

where $\tau = 0.01$ is a scalar used only to avoid null value of the denominator in Eq. 10. The subtraction of $\sigma^{2,\star}_n$ from the variance of the prediction is performed to, ideally, filter-out the noise from the training set while selecting the fidelity level to sample.

Once $\mathbf{x}^\star$ is added to the training set, the range of variation of the GP hyper-parameters $\mathbf{\Lambda}_i$ for the i-th fidelity, are bounded as: $\mathbf{\Lambda}_{i,j} = \pm\alpha\mathbf{\Lambda}^\star_{i,j-1}$, where j is the adaptive sampling iteration and $\alpha = 0.1$ is a parameter used to avoid abrupt variations of the surrogate model prediction.

3 PROBLEM STATEMENT AND SET-UP

Figure 1 shows the ASV under investigation. The SWAMP is a full-electric modular multi-functional catamaran. It can serve for various missions, such as geomorphological analysis, water sampling, physical and chemical data collection also in harsh environment. The SWAMP is conceived as collector for new research subjects like new control algorithms also for robot cooperation and testing new propulsion units [5]. The hull shape is inspired by the double-ended Wigley series and presents a flat bottom part, necessary to host the pump-jet propulsion system. The hull form and propulsion system are characterized by equally efficient sailing ahead and astern with the possibility of maneuvering in narrow spaces. The main characteristics are: overall length $L = 1.24\ m$, hull beam $B = 0.245\ m$, overall width $W = 1.1\ m$, and height $H = 0.4\ m$. The operational speed is fixed at $u = 1.0\ m/s$.

Here, the QoI is the hydrodynamic resistance R_T and the uncertain operational parameters are the vessel displacement and the position of the center of mass. The displacement ∇ (directly connected to the payload) varies depending on the type and purpose of the survey. The nominal range of variation is set as $\nabla \sim \text{unif}[35, 60]\ kg$. The center of mass x_G is positioned in the center of the hull ($x_G = 0\ m$) but can vary depending to the payload arrangement. The nominal range of variation is set as $x_G \sim \text{unif}[-0.093, 0.093]$ m (corresponding to a variation of $\pm 7.5\%$ L of the nominal value). A negative value of x_G yields a forward translation (in direction of the bow) of the center of mass, whereas a positive value yields a backward translation (in direction of the stern).

3.1 Computational Solver

The performance of the SWAMP are assessed by an in-house linear potential flow code [6]. Wave resistance computations are based on the Dawson (double-model) linearization, whereas the frictional resistance is estimated using a flat-plate approximation, based on the local Reynolds number. Finally, the hydrodynamic loads are coupled with the rigid

Figure 1: The SWAMP autonomous surface vehicle [5]

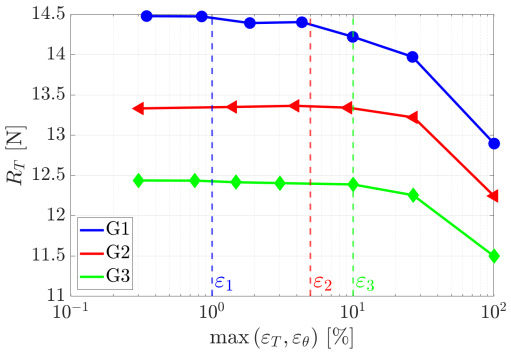

Figure 2: Total resistance versus the maximum of the percentage variations of ε_T and ε_θ for the three grids and the values of $\varepsilon_i^\star$

body equations of motion, that are solved for the sinkage (draught variation, ΔT) and trim (pitch angle variation, $\Delta\theta$), finding the equilibrium of the hydrodynamic loads acting on the hull. Under the hypothesis of small perturbations (translations and rotations) and neglecting the effects of the wave elevation, sinkage and trim are evaluated as follows

$$\Delta T \approx F_z^d/\rho g S_W, \qquad \text{and} \qquad \Delta\theta \approx M_y^d/\rho g I_W \tag{11}$$

where F_z^d is total force along the (vertical) z-axes, ρ is the density of the water, g is the gravitational acceleration, S_W is the water plane area, M_y^d is the total pitching moment, and I_W is the moment of inertia associated to the submerged part of the hull. Both M_y^d and I_W are computed with respect to the geometrical center of the hull.

The steady equilibrium between the hydrodynamic loads and the rigid body equations of motion is achieved iteratively. The equilibrium is considered achieved when

$$\max\left(\varepsilon_T, \quad \varepsilon_\theta\right) < \varepsilon^\star, \tag{12}$$

where $\varepsilon_T = |\Delta T_i - \Delta T_{i-1}|/\Delta T_i$ and $\varepsilon_\theta = |\Delta\theta_i - \Delta\theta_{i-1}|/\Delta\theta_i$ are the variations of the sinkage and trim between two subsequent iterations. The sinkage and trim variations are updated as follows: $\Delta T_i = \omega\Delta T + (1-\omega)\Delta T_{i-1}$ and $\Delta\theta_i = \omega\Delta\theta + (1-\omega)\Delta\theta_{i-1}$, with i the iteration number, $\varepsilon^\star$ the user-defined threshold, and ω an under-relaxation factor here set equal to 0.9.

3.2 Computational Set-up

The MF evaluations of the QoI are performed varying both the grid size and the value of $\varepsilon^\star$. Three fidelity levels are used, Table 1 summarizes the size of the different grids, the values of $\varepsilon^\star$, and the normalized computational cost β_i associated with each fidelity. Figure 2 shows the convergence of the total resistance versus the maximum of the percentage variations of ε_T and ε_θ for the three grids and the values chosen for $\varepsilon_i^\star$. The computational domain for the free surface is defined as $1.5L$ upstream, $3.5L$ downstream,

Table 1: Grid size, convergence threshold, and computational cost for each fidelity

i-th fidelity	Grid label	Hull panels	Free-surface panels	$\varepsilon_i^\star$ %	β_i
1	G1	6.6k	16.5k	1.00	1.000
2	G2	3.2k	8.5k	5.00	0.094
3	G3	1.5k	4.1k	10.0	0.014

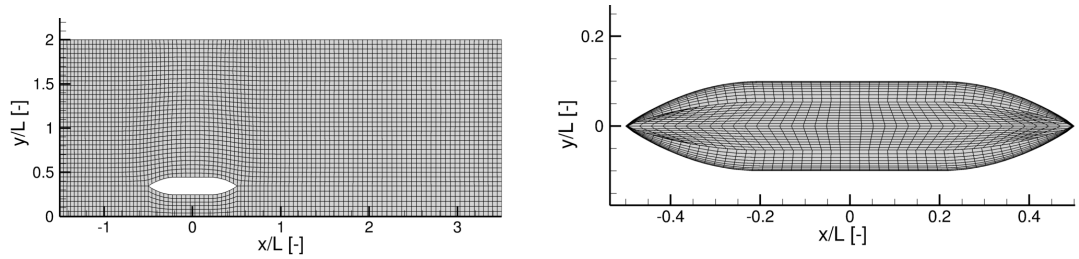

Figure 3: Computational domain and grid of the free surface (left) and the hull (right) for the G3 (low-fidelity)

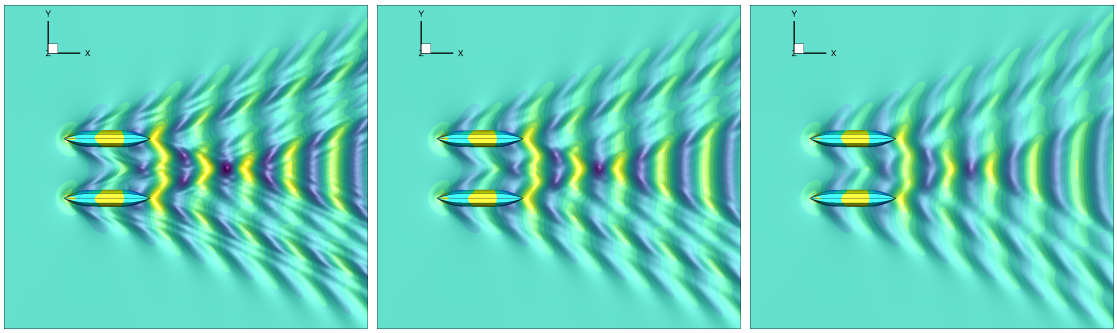

Figure 4: Wave elevations and pressure fields (from left to right G1, G2, and G3 solutions)

and $2.0L$ sideways. The computational grid G3 is shown in Fig. 3, as an example. Figure 4 shows the wave elevation and the pressure on the hull for the three grids. The wave pattern is similar for all the grids, but the local value of the wave elevation shows some differences. Differences in the pressure on the hulls can be noted in the front section.

4 NUMERICAL RESULTS

The MF-GP method is compared with its high-fidelity-based counterpart (HF-GP). A fixed computational budget, equivalent to 80 high-fidelity simulations, is used. The UQ is performed using 10,000 MC samples evaluated on the surrogate models. The expected value, variance, skewness, and kurtosis, as well the 95th percentile, and PDF of the

resistance are assessed. Furthermore, the relative errors with respect to a high-fidelity benchmark are evaluated as

$$E_i = |M_i - M_{i,\beta}|/M_{i,\beta}, \tag{13}$$

where M_i denotes the approximation of the i-th statistical moment or the 95th percentile and $M_{i,\beta}$ is the reference benchmark value. Finally, the KS test is performed [10].

The benchmark is built using a GP surrogate based on 160 HF simulations (two times the budget for the UQ). The 160 HF simulations are obtained with the adaptive sampling method based on the maximum uncertainty. The same 10,000 MC samples are used on the benchmark to evaluate the reference values of the statistical moments and the reference PDF for the KS test. The *MATLAB Statistics and Machine Learning Toolbox* [10] is used to evaluate moments, percentile, PDF, and perform the KS test.

The solution of the maximization problem in Eqs. 3 and 8 are based on a deterministic particle swarm optimization algorithm [11]. The adaptive sampling procedure starts with $2D + 1$ training points for each fidelity level, located at the domain center and at the center of the domain boundaries.

Figure 5 shows a subset of lowest fidelity training set ($\mathcal{T}_3$) for a fixed displacement $\nabla = 60$ *kg*. In the neighborhood of $x_G = 0$ *m*, there are several simulations affected by numerical noise (outliers) due to an excessively loose coupling of the hydrodynamic loads and the rigid body equations of motion. Nevertheless, the use of a regressive formulation of the GP allows to filter out the outliers.

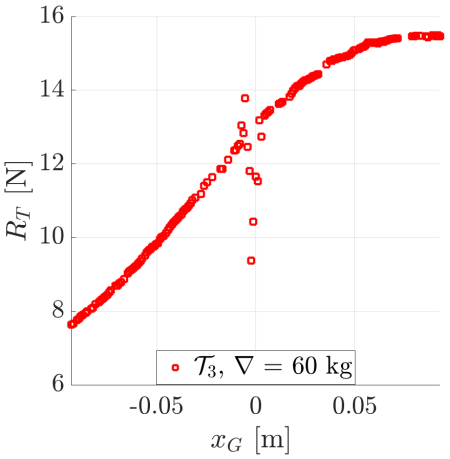

Figure 5: Outliers in the lowest fidelity training set $\mathcal{T}_3$

Figure 6 shows the response surfaces of the HF and MF GPs. The response surfaces are reported as percentage variation of the R_T with respect to the nominal value $R_{T0} = 14.35$ *N* ($\nabla_0 = 58$ *kg* and $x_G = 0$ *m*). The response surfaces are smooth and almost equal. It is worth noting that the variation of the uncertain parameters produces significant variations of R_T. The presence of the outliers seems not to affect the MF-GP response surface. The low-fidelity samples are generally uniformly distributed in the domain, although with some clusters. Finally, the MF-GP used only 52 high-fidelity simulations in comparison to 80 of HF-GP.

Figure 7 shows the convergence of the relative errors of the statistical moments for both the HF and MF GPs. Both methods achieve similar results. The HF-GP achieves slightly lower values of the error of the expected value, whereas the MF-GP achieves lower values of the error for the variance, skewness, and kurtosis. It is worth noting that the error of the expected value is below 0.1% for both HF and MF GPs, see Fig. 7a. Differently, the errors for the other statistical moments are higher, especially for the skewness. The

convergences of the MF-GP show significant oscillations (emphasized by the use of a logarithmic scale) likely due to small variations in the hyper-parameters values of the N GPs that compose the MF-GP.

Figure 8 shows the convergence of the 95th percentile error, KS statistics, and the PDF for the HF and MF GPs. The PDF is better approximated by MF-GP, especially in the interval $(7, 15)$, see Fig. 8c. This can be seen also considering the KS test statistics, where the MF-GP achieves better performance than HF-GP, see Fig. 8b. Furthermore, Fig. 8a shows that MF-GP achieves slightly better results than HF-GP in evaluating the 95th percentile.

Table 2 summarizes the reference values of the statistical moments, the 95th percentile, and the relative errors of the HF and MF GPs. Finally, it can be noted that the value of kurtosis is smaller than 3 (the kurtosis of a normal distribution) yielding a light-tailed PDF.

5 CONCLUSIONS AND FUTURE WORK

In this work an adaptive multi-fidelity Gaussian process (MF-GP) was presented for forward uncertainty quantification (UQ) of an autonomous surface vehicle: the shallow water autonomous multipurpose platform (SWAMP). The UQ was performed evaluating the first four statistical moments, the 95th percentile, and the probability density function (PDF) of the hydrodynamic resistance (R_T) of the SWAMP, subject to two uncertain operational parameters. The uncertain parameters were the displacement (directly connected to the payload) and the position of the center of mass. The UQ was performed with a Monte Carlo sampling of the response surface of the R_T as approximated by the

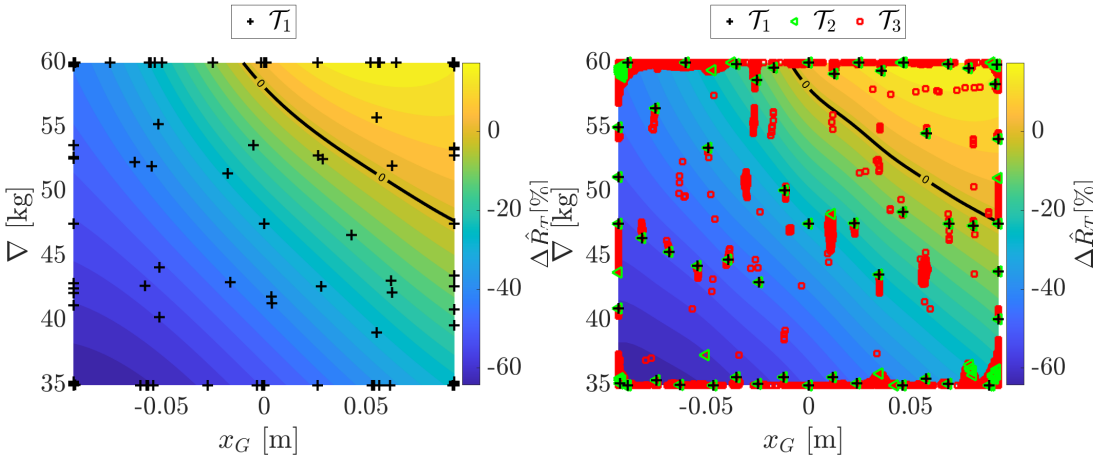

(a) High-fidelity (b) Multi-fidelity

Figure 6: GP response surfaces

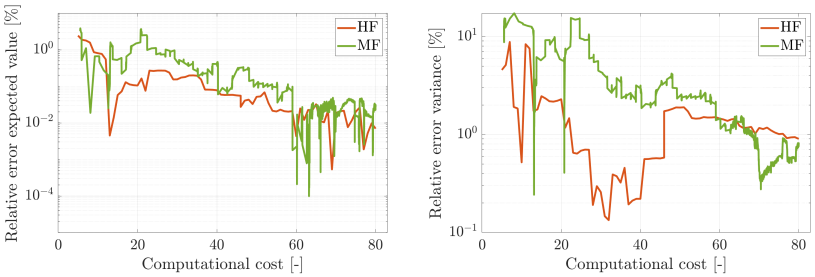

(a) Expected value (b) Variance

(c) Skewness (d) Kurtosis

Figure 7: Convergence of relative errors for the statistical moments

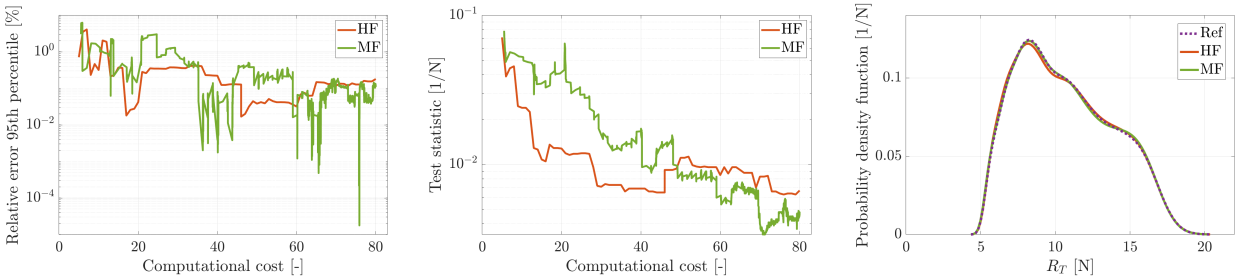

(a) Relative error of the 95th percentile (b) KS test statistic (c) PDF

Figure 8: Convergence of the 95th percentile relative error, the KS test statistics, and the PDF

MF-GP. The R_T was evaluated by a linear potential-flow solver where the hydrodynamic loads were coupled with the rigid-body equations of motion. Three levels of fidelities were used, defined by three grid sizes and tightness of the coupling between hydrodynamic and rigid-body equations of motion.

The proposed MF-GP was compared with a high-fidelity trained GP (HF-GP) at fixed computational cost. The relative errors in evaluating the statistical moments and the 95th

Table 2: Reference values of UQ, and relative errors for the high- and multi-fidelity approaches

Metric	Reference value	HF relative error%	MF relative error%
Expected value	10.65 $[N]$	**0.001**	0.027
Variance	9.596 $[N^2]$	0.954	**0.786**
Skewness	0.299 $[N^3]$	4.424	**2.026**
Kurtosis	2.022 $[N^4]$	1.272	**0.786**
95th percentile	16.13 $[N]$	0.151	**0.122**

percentile, and the Kolmogorov-Smirnov (KS) test were used to assess the performance of MF- and HF-GP. The errors were computed with respect to a high-fidelity benchmark.

The MF-GP produced a response surface identical to the one of the HF-GP while reducing by 65% the number of the high-fidelity simulations. MF-GP achieved lower values of the relative errors than HF-GP for the variance, skewness, kurtosis, and 95th percentile. The KS test showed that MF-GP was more accurate in reproducing the PDF, thus demonstrating also that the MF-GP was effective in filtering out the numerical noise in the training set.

The variation of the uncertain parameters showed significant variation of the total resistance. Specifically, the UQ showed that it is possible to reduce R_T by varying the payload position or distribution: as an example the results show that at the nominal speed of 1.00 m/s, with $\nabla = 58$ kg, it is possible to reduce by 40% the total resistance by moving forward the center of mass of $7.5\%L = 9.3cm$, see Fig. 6.

Future work will focus on keeping the penalization factor (see Eq. 10) always active, to reduce the clusterization of the training points during the adaptive sampling procedure. Furthermore, the use of a non-constant mean value in the GP formulation will be considered to improve the noise filtering capabilities of the MF-GP. Finally, the UQ analysis will be performed considering a larger number of uncertain parameters (*e.g.*, including also the advancing speed and the SWAMP width). The use of the MF-GP for higher dimensional problem is expected to produce more benefits with respect to the single-fidelity HF-GP.

ACKNOWLEDGMENTS

CNR-INM is grateful to the Italian Ministry of University and Research for the support under the Italian National Research Program PON "Ricerca e Innovazione" 2014-2020, Action II.2, Specialization area: "Blue Growth", Project n.ARS01_00682 ARES-Autonomous Robotics for the Extended Ship. CNR-INM is also grateful to Drs. Elena McCarthy and Woei-Min Lin of the Office of Naval Research for their support through the Naval International Cooperative Opportunities in Science and Technology Program.

REFERENCES

[1] Peherstorfer, B., Willcox, K., and Gunzburger, M., *Survey of multifidelity methods in uncertainty propagation, inference, and optimization.* Siam Review, (2018), 60 (3):550–591.

[2] Perdikaris, P., Venturi, D., Royset, J. O., and Karniadakis G. E., *Multi-fidelity modelling via recursive co-kriging and gaussian–markov random fields.* Proceedings of the Royal Society A: Mathematical, Physical and Engineering Sciences, (2015), 471(2179):20150018.

[3] Brevault, L., Balesdent, M., and Hebbal, A., *Overview of gaussian process based multi-fidelity techniques with variable relationship between fidelities, application to aerospace systems.* Aerospace Science and Technology, (2020), 107:106339.

[4] Liu, Y., Shi, Y., Zhou, Q., and Xiu, R., *A sequential sampling strategy to improve the global fidelity of metamodels in multi-level system design.* Structural and Multidisciplinary Optimization, (2016), 53 (6): 1295–1313.

[5] Odetti, A., Bruzzone, G., Altosole, M., Viviani, M., and Caccia, M., *SWAMP, an Autonomous Surface Vehicle expressly designed for extremely shallow waters*, Ocean Engineering 216, (2020): 108205.

[6] Bassanini, P., *The wave resistance problem in a boundary integral formulation*, Surv Math Ind, (1994), Vol. 4 pp. 151-194.

[7] Serani, A., Pellegrini, R., Wackers, J., Jeanson, C.-E., Queutey, P., Visonneau, M., and Diez, M., *Adaptive multi-fidelity sampling for CFD-based optimisation via radial basis function metamodels*, International Journal of Computational Fluid Dynamics, (2019), Vol. 33, No. 6-7, pp. 237–255.

[8] Williams, C. K., and Rasmussen, C. E., *Gaussian processes for machine learning*, MIT press Cambridge, MA (2006), Vol. 2.

[9] Wackers, J., Visonneau, M., Ficini, S., Pellegrini, R., Serani, A., and Diez, M., *Adaptive N-Fidelity Metamodels for Noisy CFD Data*, AIAA AVIATION 2020 FORUM, (2020), p. 3161.

[10] MATLAB and Statistics Toolbox Release 2021a, Version 12.1, The MathWorks, Inc. (2021).

[11] Serani, A., Leotardi, C., Iemma, U., Campana, E. F., Fasano, G., and Diez, M., *Parameter selection in synchronous and asynchronous deterministic particle swarm optimization for ship hydrodynamics problems*, Applied Soft Computing, (2016), Vol. 49, pp. 313 – 334.